Redox Biology 30 (2020) 101418

Contents lists available at ScienceDirect

Redox Biology

journal homepage: www.elsevier.com/locate/redox

Research Paper

Dihydrolipoamide dehydrogenase regulates cystine deprivation-induced ferroptosis in head and neck cancer

Daiha Shin[a,b,1], Jaewang Lee[a,1], Ji Hyeon You[a], Doyeon Kim[a], Jong-Lyel Roh[a,*]

[a] Department of Otorhinolaryngology-Head and Neck Surgery, CHA Bundang Medical Center, CHA University School of Medicine, Seongnam, Republic of Korea
[b] Western Seoul Center, Korea Basic Science Institute, Seoul, Republic of Korea

ARTICLE INFO

Keywords:
Ferroptosis
Dihydrolipoamide dehydrogenase
Mitochondria
Cystine deprivation
Iron

ABSTRACT

Ferroptosis is a new form of regulated cell death driven by iron-dependent lipid peroxidation. Glutaminolysis and tricarboxylic acid cycle are involved in ferroptosis, but the underlying metabolic process remains unclear. We examined the role of dihydrolipoamide dehydrogenase (DLD) in ferroptosis induction in head and neck cancer (HNC). The effects of cystine deprivation or sulfasalazine treatment and of DLD gene silencing/overexpression were tested on HNC cell lines and mouse tumor xenograft models. These effects were analyzed with regard to cell death, lipid reactive oxygen species (ROS) and mitochondrial iron production, mitochondrial membrane potential, mRNA/protein expression, and α-ketoglutarate dehydrogenase (KGDH)/succinate/aconitase activities. Cystine deprivation induced ferroptosis via glutaminolysis. Cystine deprivation or import inhibition using sulfasalazine induced cancer cell death and increased lipid ROS and mitochondrial iron levels, which had been significantly decreased by short-interfering RNA (siRNA) or short hairpin RNA (shRNA) targeting DLD ($P < 0.01$) but not by dihydrolipoyl succinyltransferase. The same results were noted in an *in vivo* mouse model transplanted with vector or shDLD-transduced HN9 cells. After cystine deprivation or sulfasalazine treatment, mitochondrial membrane potential, mitochondrial free iron level, KGDH activity, and succinate content significantly increased ($P < 0.001$), which had been blocked by DLD siRNA or shRNA and were consequently rescued by resistant DLD cDNA. Cystine deprivation caused iron starvation response and mitochondrial iron accumulation for Fenton reaction and ferroptosis. Our data suggest a close association of DLD with cystine deprivation- or import inhibition-induced ferroptosis.

1. Introduction

Ferroptosis is a new form of regulated necrosis, which is driven by iron-dependent lipid peroxidation [1]. The initial molecular circuitries engage in the depletion of glutathione (GSH), which is a major cellular antioxidant, by causing cystine deprivation or inhibiting the system x_c^- cystine/glutamate antiporter (xCT) [1]. Glutathione peroxidase (GPX4), an essential regulator of ferroptosis, suppresses lipid peroxidation generation and ferroptosis [2,3]. Specific agents that either induce (e.g., erastin, sulfasalazine, RSL3, and FIN56) or inhibit (e.g., ferrostatins, liprostatins, and vitamin E) ferroptosis can modulate the regulated cell death process by targeting xCT and GPX4 [1]. Ferroptosis also involves preferential oxidation of polyunsaturated fatty acids (PUFAs) [4,5] and Fenton reaction via increased intracellular iron degradation and ferritinophagy [6,7]. The Nomenclature Committee on Cell Death 2018 has newly included ferroptosis as a form of regulated cell death, which is initiated by intracellular oxidative and iron perturbations that can in turn be inhibited by lipophilic antioxidants and iron chelators [8]. There is growing evidence that ferroptosis can be useful for effectively killing cancer cells while leaving the normal cells intact, particularly in acquired resistant, immune-evading cancer cells [9,10].

Lethal lipid peroxidation disturbs the integrity of cellular plasma membrane during ferroptosis, plausibly in the mitochondria, endoplasmic reticulum, and lysosomes [11]. Mitochondria plays a central role in oxidative metabolism by generating cellular reactive oxygen species (ROS) and radicals, which damage cellular components, via respiratory chains [12]. Whether mitochondria is essential in a ferroptotic process remains unclear because induction of necrotic cell death occurred even in mitochondrial-deficient cells [13]. However,

* Corresponding author. Department of Otorhinolaryngology-Head and neck Surgery, CHA Bundang Medical Center, CHA University, Seongnam, Gyeonggi-do, 13496, Republic of Korea.
E-mail address: rohjl@cha.ac.kr (J.-L. Roh).
[1] The first two authors (D.S. and J. L.) equally contributed to this manuscript.

https://doi.org/10.1016/j.redox.2019.101418
Received 19 November 2019; Received in revised form 16 December 2019; Accepted 29 December 2019
Available online 07 January 2020

Abbreviations

ACO	aconitase
αKG	α-ketoglutarate
CC	cystine
DLD	dihydrolipoamide dehydrogenase
DLST	dihydrolipoyl succinyltransferase
ETC	electron transfer chain
Fpn	ferroportin
GLS	glutaminase
GPX4	glutathione peroxidase 4
GSH	glutathione
HNC	head and neck cancer
ISC	iron-sulfur cluster
IRP2	iron regulatory protein 2
KGDH	α-ketoglutarate dehydrogenase
MDA	malondialdehyde
MMP	mitochondrial membrane potential
NADH	a reduced form of nicotinamide adenine dinucleotide
PI	propidium iodide
ROS	reactive oxygen species
RPA	rhodamine B-[(1,10-phenanthroline-5-yl)-aminocarbonyl] benzyl ester
siRNA	short-interfering RNA
shRNA	short hairpin RNA
TCA	tricarboxylic acid
SAS	sulfasalazine
TfR	transferrin receptor protein
TMRE	tetramethylrhodamine ethyl ester
xCT	system x_c^- cystine/glutamate antiporter

ferroptosis causes distinguished morphological changes, namely mitochondrial fragmentation, cristae enlargement, and membrane rupture, but retains the structural integrity of nucleus [5]. Additionally, fueling of the tricarboxylic acid (TCA) cycle via glutaminolysis is required for inducing lipid peroxidation and ferroptosis by cysteine deprivation or import inhibition [14].

The pivotal role of mitochondria in ferroptosis has been recently confirmed after a study demonstrated the association of glutaminolysis, electron transfer chain (ETC), and TCA cycle with cysteine deprivation-induced ferroptosis [15]. Cysteine deprivation is associated with ETC activity and hyperpolarization of mitochondrial membrane potential (MMP), which might be dispensable for ferroptosis induced by GPX4 inhibition [15]. Cancer cells may confer resistance to ferroptosis via loss-of-function mutation of the tumor suppressor, fumarate hydratase, which is involved in the TCA cycle [16]. Glutaminolysis and TCA cycle are involved in ferroptosis, but the underlying metabolic process remains unclear. The present study has newly found a close relationship between dihydrolipoamide dehydrogenase (DLD) and ferroptosis induced by cystine deprivation or import inhibition. Here, we examined the role of DLD in the induction of ferroptosis.

2. Materials and methods

2.1. Cell culture and reagents

HNC cell lines, namely AMC HN3, HN4, and HN9 [17], were used after authentication by short tandem repeat-based DNA fingerprinting and multiplex polymerase chain reaction (PCR). The cells were cultured in Eagle's minimum essential medium (Thermo Fisher Scientific, Waltham, MA, USA) supplemented with 10% fetal bovine serum at 37 °C in a humidified atmosphere containing 5% CO_2. The cells were also cultured in a conditioned media without cystine and cysteine and were subsequently exposed to sulfasalazine (Sigma-Aldrich, St. Louis, MO, USA) for indicated time and dose.

2.2. Cell death assays

Cell death occurring after the cells were subjected to cystine deprivation or sulfasalazine treatment for indicated time was assessed via PI staining. Control cells were exposed to an equivalent amount of dimethyl sulfoxide (DMSO). The sample is washed twice with PBS, followed by staining of cells in each plate with 2.5 μg/mL PI (Sigma-Aldrich) in PBS for 30 min. The stained cells were analyzed using a FACSCalibur flow cytometer equipped with CellQuest Pro (BD Biosciences, San Jose, CA, USA) and observed using a ZEISS fluorescent microscope (Oberkochen, Germany). The mean PI-positive fractions were compared with those of the control group.

2.3. Measurement of GSH synthesis, ROS production, and lipid peroxidation

Intracellular GSH levels in HNC cell lysates subjected to cystine deprivation for 8 h were measured using a GSH colorimetric detection kit (BioVision Inc., Milpitas, CA, USA). After cystine deprivation or sulfasalazine treatment for 2–10 h, cellular ROS generation in the supernatant of HNC cell lysates was measured by adding 10 μM 2′,7′-dichlorofluorescein diacetate (DCF-DA) (cytosolic ROS; Enzo Life Sciences, Farmingdale, NY, USA) or 2 μM C11-BODIPY C11 (lipid peroxidation; Thermo Fisher Scientific) for 30 min at 37 °C. The ROS levels were analyzed using a FACSCalibur flow cytometer equipped with CellQuest Pro (BD Biosciences). Cellular lipid peroxidation was assessed in HNC cell lysates by measuring the concentration of MDA, an end product of lipid peroxidation, using a lipid peroxidation assay kit (Abcam, Cambridge, MA, USA).

2.4. Mitochondrial iron, superoxide generation, and membrane potential assays

Mitochondria were isolated using the mitochondrial isolation kit (Thermo Fisher Scientific). Ferrous iron level in the cell or mitochondria was measured using the iron assay kit (Sigma-Aldrich). The accumulation of intra-mitochondrial iron was also measured with rhodamine B-[(1,10-phenanthroline-5-yl)-aminocarbonyl]benzyl ester (RPA), a fluorescent non-toxic iron sensor (Squarix GmbH, Marl, Germany). Arbitrary fluorescence units (AUs) were compared among differently treated groups. MMP were measured by staining the cells with 200 nM tetramethylrhodamine ethyl ester (TMRE, Thermo Fisher Scientific) for 20 min. The mean fluorescent intensity of each group was normalized to that of the control group.

2.5. RNA interference and gene transfection

For silencing the *DLD* gene, HN9 cells were seeded. Cells were transfected 24 h later with 10 nmol/L small-interfering RNA (siRNA) targeting human *DLD* or scrambled control siRNA (Integrated DNA Technologies, Coralville, IA, USA). The HN9 cells were stably transduced with shRNA targeting DLD (Integrated DNA Technologies). To generate cells that stably overexpress *DLD*, HN9 cells were stably transfected with a control plasmid (pBABE-puro, Addgene, Watertown, MA, USA) or a resistant *DLD* (DLDres, gBocks® gene fragment DLD, Integrated DNA Technologies)-cloned plasmid. *DLD* expression was confirmed via western blotting performed using anti-DLD antibody.

2.6. Reverse transcription-quantitative PCR and immunoblotting

Cells were plated and grown with 70% confluence, and then

subjected to treatment with the indicated drugs. Total RNA from HNC cells was extracted using an RNA extraction kit (ThermoFisher Scientific) according to the manufacturer's instructions. A reverse transcription-quantitative PCR from 1 to 2 μg total RNA for each extracted sample was conducted using SensiFAST™ SYBR® No-ROX Kit (Bioline International, Toronto, Canada) after performing cDNA synthesis using SensiFAST™ cDNA Synthesis Kit (Bioline International). *IREB2, TFRC, SLC40A1*, and *ACTB* were amplified, and the relative target mRNA levels were determined using the $2^{-(\Delta\Delta Ct)}$ method and normalized against *ACTB* mRNA levels.

For immunoblotting, cells were lysed at 4 °C in a cell lysis buffer (Cell Signaling Technology, Danvers, MA, USA) with protease/phosphatase inhibitor cocktail (Cell Signaling Technology). A total of 5–15 μg protein was resolved by SDS-PAGE on 10%–15% gels; the resolved proteins were then transferred to nitrocellulose or polyvinylidene difluoride membranes and probed with primary and secondary antibodies. The following primary antibodies were used: DLD (GTX101245; GeneTex Inc., Irvine, CA, USA), DLST (11954S; Cell Signaling Technology), ACO1 (ab126595, Abcam), ACO2 (ab110321, Abcam), and iron regulatory protein (IRP) 2 (sc-33682, Santa Cruz Biotechnology, Inc., Dallas, TX, USA). β-actin (BS6007 M, BioWorld, Atlanta, GA, USA) served as the total loading control. All antibodies were diluted to concentrations between 1:500 and 1:10000.

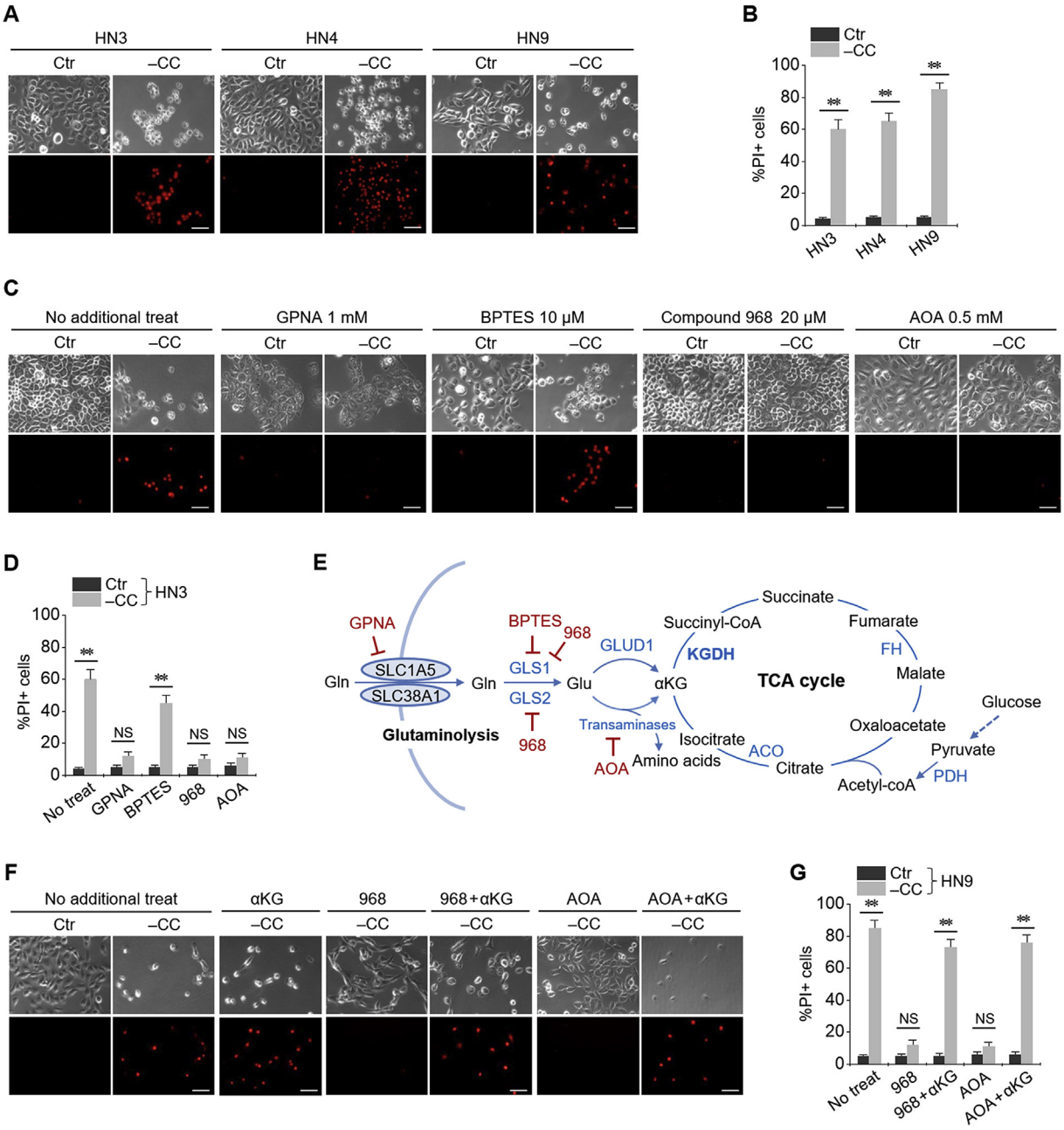

Fig. 1. Glutaminolysis mediates cystine deprivation-induced ferroptosis. (***A, B***) Ferroptotic cell death induced by cystine (CC) deprivation in head and neck cancer (HNC) cells. Propidium iodide (PI)-positive cells were stained and counted using fluorescent microscopy and flow cytometry after cystine deprivation for 48 h. (***C, D***) Pharmacological inhibition of glutaminolysis pathway abrogating ferroptotic cell death. (***E***) Schematic summary of the glutaminolysis pathway and tricarboxylic acid (TCA) cycle. (***F***) α-ketoglutarate (αKG) mimicking ferroptotic cell death mediated by glutaminolysis. Four millimolar αKG was added to the media with or without 20 μM Compound 968 or 0.5 mM AOA. Scale bar, 50 μm $^{**}P < 0.001$. NS indicates statistically not significant.

2.7. Assays for analyzing KGDH, succinate, and aconitase activities

The α-ketoglutarate dehydrogenase (KGDH) activities and succinate contents were examined in HN9 cells subjected to cystine deprivation or sulfasalazine treatment for 4 or 8 h, according to the manufacturer's protocol of KGDH assay kit (K678-100, BioVision Inc.) and succinate colorimetric assay kit (K649-100, BioVision Inc.), respectively. Aconitase activity was also measured in HN9 cells with or without shDLD, DLDres, or vector using an aconitase activity colorimetric assay kit (K716-100, BioVision Inc.).

2.8. Tumor xenograft

All animal study procedures were performed in accordance with protocols approved by the Institutional Animal Care and Use Committee (IACUC). Six-week-old athymic BALB/c male nude mice (nu/nu) were purchased from Central Lab Animal Inc. (Seoul, Republic of Korea). HN9 cells with shDLD or vector control were subcutaneously injected into the bilateral flank of nude mice. From the day when gross nodules were detected in tumor implants, mice were subjected to different treatments: vehicle or sulfasalazine (250 mg/kg daily per intraperitoneal route) [18]. Each group included seven mice. Tumor size and body weight of each mice were measured twice a week, and tumor volume was calculated as (length × width^2)/2. After scarification of mice, tumors were isolated and analyzed by measuring cellular lipid ROS and mitochondrial iron contents. AUs were compared among differently treated tumors.

2.9. Statistical analysis

Data were presented as mean ± standard error of mean. The statistically significant differences between the treatment groups were assessed using Mann–Whitney *U* test or analysis of variance (ANOVA) with Bonferroni post-hoc test. The expression levels of DLD mRNA were obtained from the normal mucosa (n = 43) and HNC (n = 519) datasets of TCGA assessed from the cBioPortal (www.cbioportal.org). The median values of low and high expression levels of DLD mRNA were determined and compared using *t*-test. Univariate Cox proportional

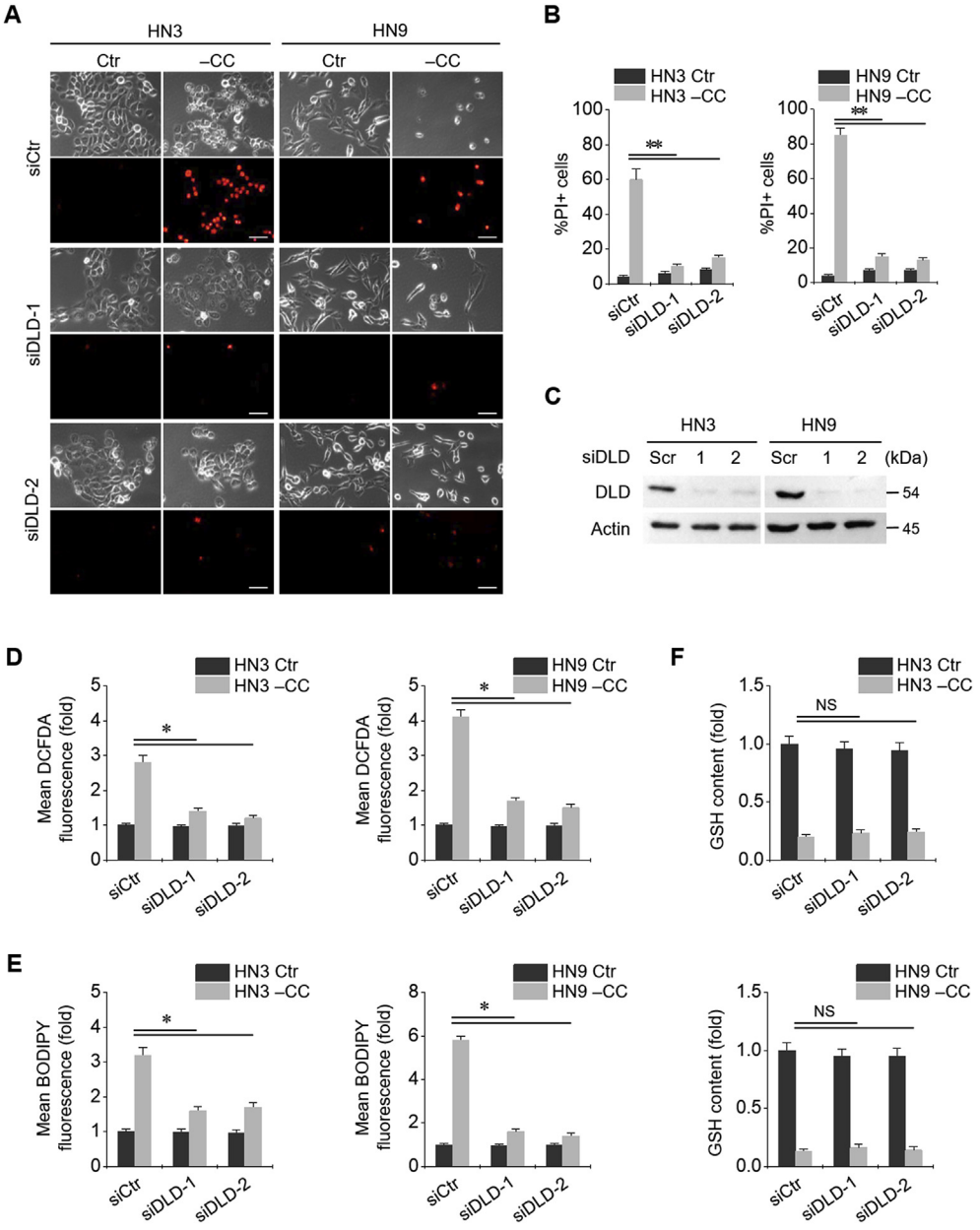

Fig. 2. Dihydrolipoamide dehydrogenase (DLD) is associated with ferroptotic cell death induced by cystine deprivation. (***A–C***) Silencing of DLD gene in HN3 and HN9 cell lines. PI-positive cells were stained and counted using fluorescent microscopy and flow cytometry after cystine deprivation for 48 h. Scale bar, 50 μm $^{**}P < 0.001$ relative to scrambled siRNA control (siCtr). Western blotting was performed for these cells at 24 h after siDLD or siCtr transfection. (***D–E***) Cellular reactive oxygen species (ROS) and glutathione (GSH) contents and lipid ROS in HN3 and HN9 cells, with or without DLD gene silencing, which were subjected to CC deprivation for 8 h $^{*}P < 0.01$ relative to siCtr. NS indicates statistically not significant.

hazards regression analyses were used to identify associations between DLD mRNA expression levels and overall survival or disease-free survival in the HNC cohort. The Kaplan–Meier and log-rank tests were used to determine and statistically compare the survival rates, respectively. All statistical tests were two-sided and a P value of < 0.05 was considered to be statistically significant. The statistical tests were performed using IBM® SPSS® Statistics version 24.0 for Windows (IBM, Armonk, NY, USA).

3. Results

3.1. Glutaminolysis mediates cystine deprivation-induced ferroptosis

Cystine deprivation induced ferroptotic cell death in head and neck (HNC) cell lines. Propidium iodide (PI)-positive cell fraction considerably increased in HN3, HN4, and HN9 cancer cells with cystine deprivation (Fig. 1A and B). When multiple components involved in the glutaminolysis pathway were pharmacologically inhibited, the ferroptotic cell death was significantly prevented except when co-treated with BPTES, a GLS1 inhibitor ($P < 0.001$) (Fig. 1C–E). However, the extent of suppression of cell death by Compound 968, which inhibits both GLS1 and GLS2, significantly increased owing to cystine deprivation. GPNA (SLC1A5 inhibitor) and AOA (pan-transaminases inhibitor) also suppressed cystine deprivation-induced ferroptosis. The final product of glutaminolysis pathway, α-ketoglutarate (αKG), re-induced ferroptotic cell death inhibited by Compound 968 or AOA during the scenario of cystine deprivation (Fig. 1F and G).

3.2. DLD links to ferroptosis induced by cystine deprivation or import inhibition

Cystine deprivation led to an increase in the cell death of HNC cells. PI-positive cell fraction significantly increased in HN3 and HN9 cells with cystine deprivation (Fig. 2A and B). When siDLD was transfected in both HNC cell lines, the protein expression of DLD significantly decreased ($P < 0.001$) (Fig. 2C). Along with DLD gene silencing, the PI-positive fraction in cystine-deprived cells decreased nearly up to that in controls (cells without cystine deprivation). Cystine deprivation induced a significant increase in cellular and lipid ROS and caused depletion of GSH (Fig. 2D–F). DLD gene silencing caused a significant reduction in cellular and lipid ROS levels induced by cystine deprivation but did not change intracellular GSH contents.

Stable transduction of DLD shRNA and vector was established in HN9 cells. Cystine deprivation or treatment with sulfasalazine, an inhibitor of xCT, induced ferroptotic cell death of HN9 cells. DLD gene silencing significantly reduced PI positivity and lipid ROS in HN9 cells induced by cystine deprivation or 1 mM sulfasalazine treatment ($P < 0.001$) (Fig. 3A–C). Stable transduction of resistant DLD cDNA (DLDres) modestly increases PI positivity in HN9 cells subjected to cystine deprivation or sulfasalazine treatment (Fig. 3D and E). In

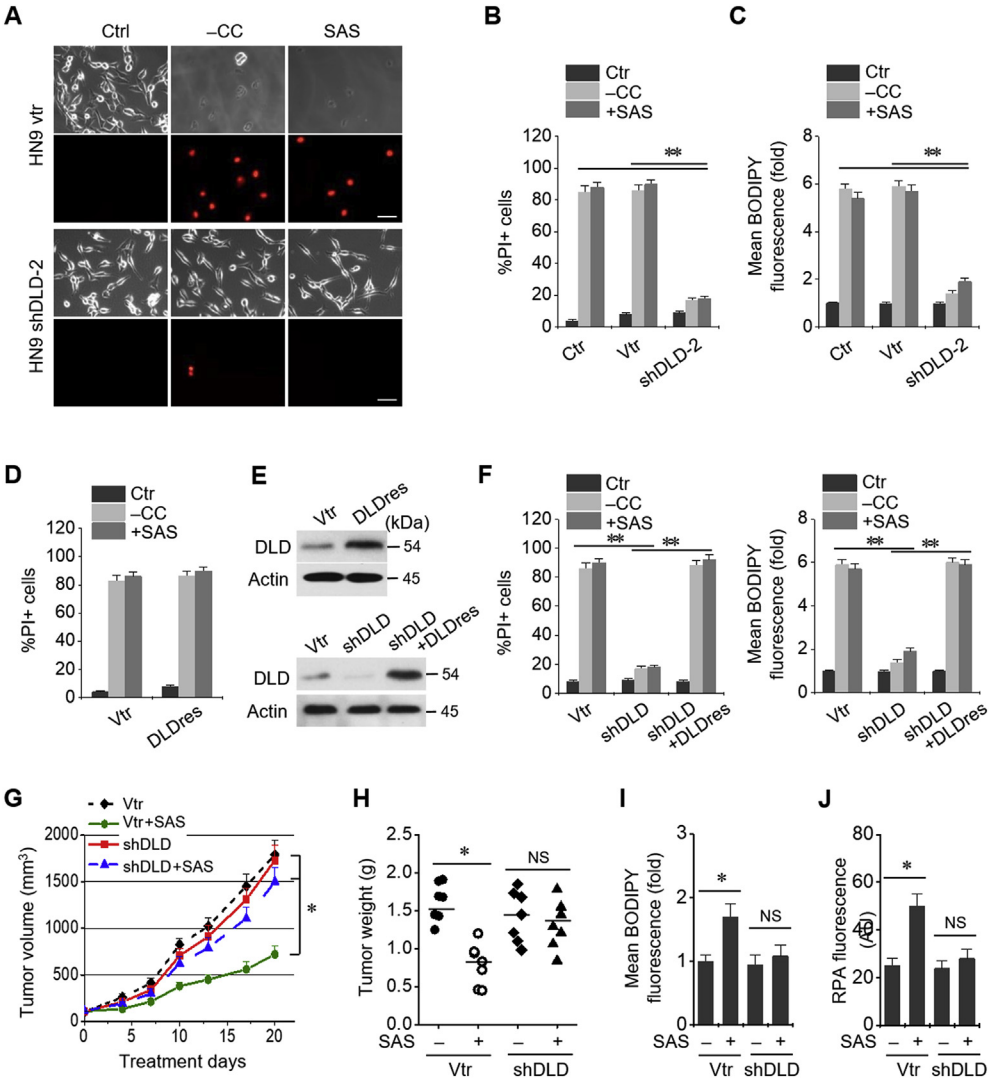

Fig. 3. DLD regulates ferroptosis induced by cystine deprivation or import inhibition. (***A–C***) Cell death and lipid ROS assays in HN9 cells stably transduced with shRNA targeting DLD or a vector control (vtr). The cells were subjected to CC deprivation or 1 mM sulfasalazine (SAS) treatment for 48 h (PI-positive cells) or 8 h (BODIPY fluorescence). Scale bar, 50 μm $^{**}P < 0.001$ relative to vtr or control without vector or shDLD (ctr). (***D–F***) Cell death and lipid ROS in HN9 cells stably transduced with a resistant DLD cDNA (DLDres), shDLD, or a vector control. PI and BODIPY were stained and counted using flow cytometry after the cells were subjected to CC deprivation or 1 mM SAS treatment for 48 h and 8 h, respectively. Western blots were performed in these cells stably transduced with DLDres, shDLD, or vector. $^{**}P < 0.001$ relative to a vector control. (***G–J***) Effects of DLD gene silencing on SAS-induced inhibition of tumor growth *in vivo*. Tumor volumes were regularly measured after SAS or vehicle treatments in nude mice implanted with shDLD or vtr-transduced HN9 cells. Lipid ROS level and mitochondrial iron accumulation in tumors were measured using BODIPY and rhodamine B-[(1,10-phenanthroline-5-yl)-aminocarbonyl]benzyl ester (RPA). $^{*}P < 0.01$ relative to control. NS indicates statistically not significant.

addition, the expression of DLDres completely rescued the reduction of PI positivity and lipid ROS induced by shDLD in HN9 cells subjected to cystine deprivation or sulfasalazine treatment (Fig. 3F). Effects of DLD gene silencing on sulfasalazine-induced inhibition of tumor growth was examined in nude mice transplanted with HN9 cells stably transduced with shDLD or vector. Sulfasalazine treatment inhibited the tumor growth *in vivo*, which was significantly reduced in HN9 cells with shDLD ($P < 0.01$) (Fig. 3G and H). Lipid ROS and mitochondrial iron accumulated in vector-controlled tumors treated with sulfasalazine but not in shDLD-transduced tumors (Fig. 3I and J).

3.3. MMP hyperpolarization and KGDH activity are associated with ferroptosis

Mitochondrial membrane potential (MMP) and lipid ROS increased along times elapsed with maximum around 8 h after cystine deprivation or sulfasalazine treatment (Fig. 4A and B); however, MMP and lipid ROS were significantly suppressed by shDLD and completely rescued by DLDres ($P < 0.001$). KGDH activities and relative succinate content also increased along with cystine deprivation or sulfasalazine treatment, which had been significantly inhibited by shDLD and were rescued by DLDres ($P < 0.01$) (Fig. 4C and D). Gene silencing of dihydrolipoyl succinyltransferase (DLST), which is the E2 unit of KGDH complex, did not block cystine deprivation-induced ferroptosis as that observed in case of DLD gene silencing (Fig. 4E–G).

3.4. Cystine deprivation causes iron starvation response and mitochondrial iron accumulation

Mitochondrial malondialdehyde (MDA) and ferrous ion (Fe^{2+}) levels increased in HNC cells subjected to cystine deprivation or sulfasalazine treatment (Fig. 5A and B). Intra-mitochondrial RPA fluorescence also increased in these conditions (Fig. 5C). Mitochondrial MDA, Fe^{2+}, and RPA levels had been significantly inhibited by shDLD and

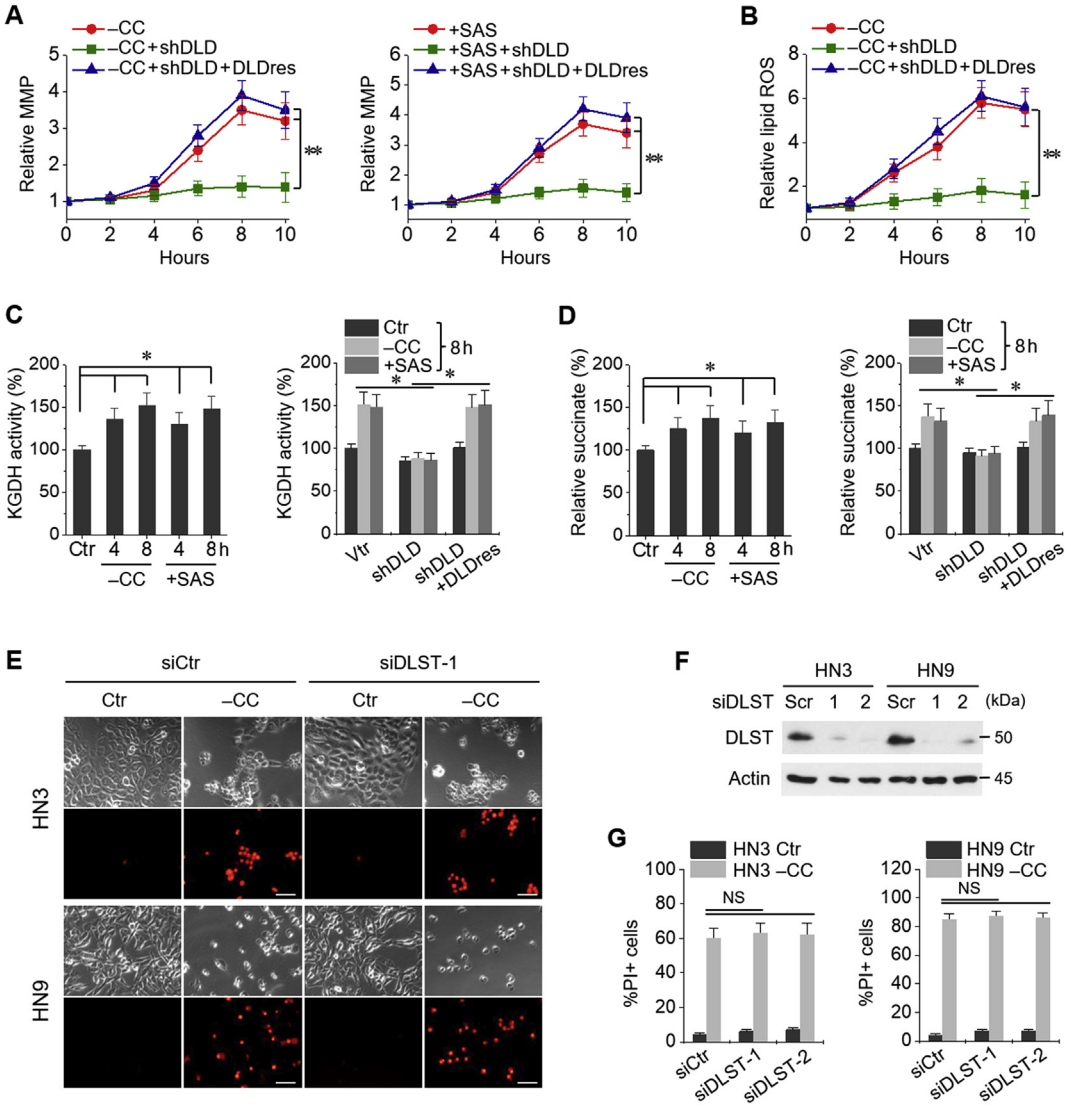

Fig. 4. Mitochondrial membrane potential (MMP) and α-ketoglutarate dehydrogenase (KGDH) activities are associated with ferroptosis. (***A***, ***B***) MMP and lipid ROS changes in HN9 cells stably transduced with shDLD, DLDres, or a vector control (vtr). The cells were subjected to CC deprivation or 1 mM SAS at different time points, and then, MMP and lipid ROS were incubated with tetramethylrhodamine ethyl ester (TMRE, 200 nM) and BODIPY, respectively, 30 min before each indicated time point. $^{**}P < 0.001$ relative to a vector control or shDLD plus DLDres. (***C***, ***D***) Quantification of KGDH activity and succinate in HN9 cells stably transduced with shDLD, DLDres, or vtr. The cells were also exposed to CC deprivation or 1 mM SAS for 4 or 8 h $^{*}P < 0.01$ relative to control or between different groups with or without shDLD or DLDres. (***E–G***) Cell death assay in HN3 and HN9 cells with or without dihydrolipoyl succinyltransferase (DLST) gene silencing. The cells were transfected with siDLST or scrambled siRNA (siCtr) and then subjected to CC deprivation. Western blots were performed in the cells with siDLST or siCtr. Scale bar, 50 μm. NS indicates statistically not significant.

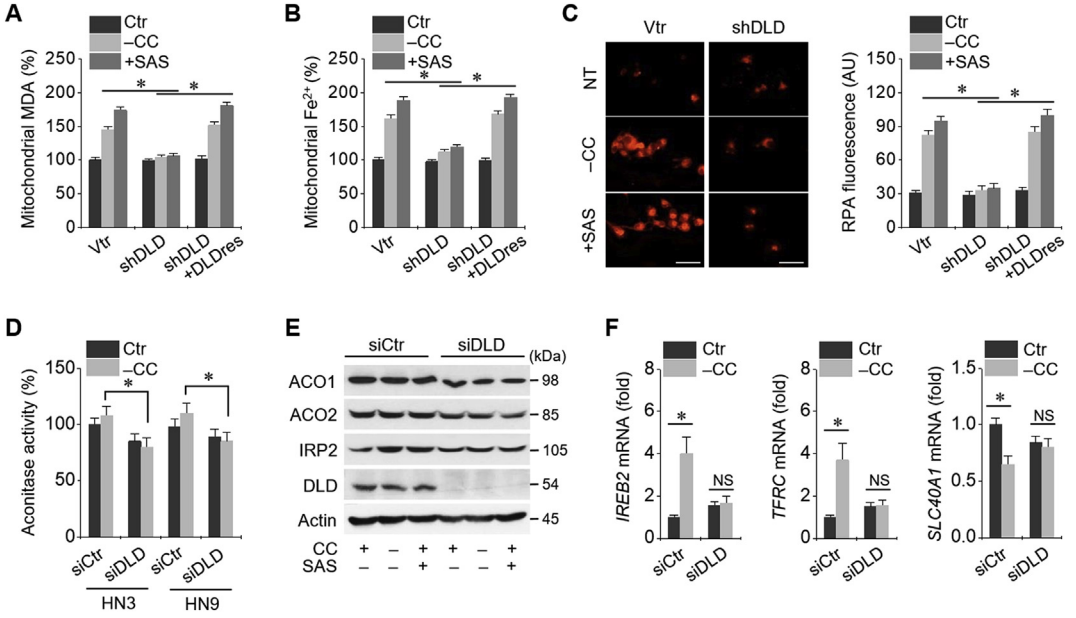

Fig. 5. Cystine deprivation causes iron starvation response and mitochondrial iron accumulation for Fenton reaction. (***A***, ***B***) Mitochondrial malondialdehyde (MDA) and ferrous ion (Fe^{2+}) levels were assayed in HN9 cells stably transduced with vtr, shDLD, or DLDres, and then, these cells were subjected to CC deprivation or 1 mM SAS treatment for 8 h. (***C***) Accumulation of RPA in these cells subjected to CC deprivation or 1 mM SAS treatment for 8 h. Scale bar, 50 μm. (***D–F***) Aconitase activity, protein levels of aconitase (ACO) 1 and 2, iron regulatory protein 2 (IRP2), and DLD, and mRNA levels of IRP2 (IREB2), transferrin receptor protein 1 (TfR1, *TFRC*), and Fpn-1 (*SLC40A1*) genes in HN-3 cells with siCtr or siDLD transfection. *$P < 0.01$ between siCtr and siDLD. NS indicates statistically not significant.

rescued by DLDres ($P < 0.01$). Aconitase activity increased owing to cystine deprivation, but this increase was not statistically significant ($P > 0.05$); however, the activity was significantly higher than that in HNC cells with DLD gene silencing ($P > 0.01$) (Fig. 5D). IRP2 protein level increased in HN3 cells subjected to cystine deprivation or sulfasalazine treatment, but ACO1 and ACO2 protein levels remained relatively unchanged (Fig. 5E). IRP2 and TfR1 mRNA levels significantly increased but Fpn-1 mRNA and protein levels significantly decreased because of cystine deprivation ($P < 0.01$), which was not observed in HN3 cells with DLD gene silencing (Fig. 5F). Taken together, these findings suggested that iron starvation response and mitochondrial iron accumulation occurred as a result of cystine deprivation.

3.5. DLD mRNA expression level in and survival of HNC cells

From the TCGA datasets, it was found that mean (± standard deviation) expression level of DLD was significantly lower in the HNC samples than in normal ones (10.75 ± 0.51 vs. 11.22 ± 0.50; $P < 0.001$). Median (interquartile range) values of DLD mRNA expression were 10.73 (10.45–11.01) in 519 HNC samples and 11.11 (10.94–11.47) in 43 normal samples (Fig. 6A). High and low expression levels of DLD mRNA in HNC samples were determined by the median values in the HNC cohort from the TCGA datasets. Univariate Cox proportional hazard regression analysis showed that the expression level of DLD mRNA was not significantly associated with overall survival or disease-free survival outcomes ($P > 0.5$) (Fig. 6B and C).

4. Discussion

Glutaminolysis is linked with the regulation of ferroptosis in cancer cells. Glutamine is a conditionally essential amino acid abundantly present in human tissues and plasma. Tumor cells show glutamine dependency owing to the need for glutaminolysis fueling to carry out the TCA cycle and essential biosynthetic processes supporting tumor growth [19]. Glutaminolysis replenishes the TCA cycle intermediates that play a role in cystine deprivation- or import inhibition-induced ferroptosis and provide sources for tumor growth [14,15]. Cystine deprivation or import inhibition fails to induce lipid ROS accumulation

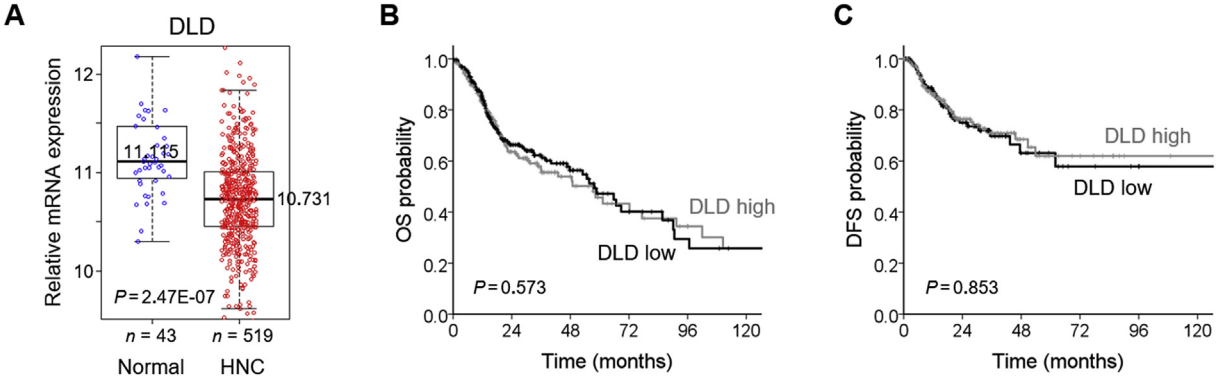

Fig. 6. DLD mRNA expression level in and survival of the HNC cohort of the TCGA datasets. (***A***) Comparison of DLD mRNA levels between 43 normal mucosa samples and 519 HNC samples. The bar values indicated median. (***B***, ***C***) Kaplan–Meier curves estimating overall survival (OS) and disease-free survival (DFS) according to low and high expression levels of DLD mRNA in the HNC patient cohort of the TCGA datasets. Log-rank test was used to compare the survival rates between groups.

and ferroptosis when glutaminolysis is inhibited [14,15]. In the present and previous studies [14], ferroptosis might be abrogated by the blockade of the components involved in glutaminolysis, namely SLC1A5 and SLC38A1 (glutamine transport), GLS1 and GLS2 (glutaminase, glutamine to glutamate), and transaminase and GLUD1 (from glutamate to αKG). GLS2, but not GLS1, reportedly played a critical role in glutaminolysis, and thereby contributed to ferroptosis; GLS2 is also a transcriptional target of p53 and its upregulation contributes to p53-depedent cell death [20]. In the absence of glutamine or inhibition of glutaminolysis, cystine deprivation could not induce ferroptosis; this phenomenon could be reversed by the addition of αKG, as shown in the present and previous studies. Taken together, the anaplerotic reaction via glutaminolysis might be required for cystine deprivation-induced ferroptosis.

The present study showed that DLD was closely associated with ferroptosis induced by cystine deprivation or import inhibition. DLD and DLST constitute the E3 and E2 components of KGDH complex, respectively, that is deeply interconnected with mitochondrial ETC and regulates cellular redox state [21]. Production of αKG via glutaminolysis can fuel both energetic and anabolic pathways executed by the KGDH complex inside the mitochondria. Thus, our study further implies that MMP and KGDH activity mediated by glutaminolysis are associated with ferroptosis. Increased αKG level stimulates DLD to generate hydrogen peroxides in response to the accumulation of NADH, which is a reduced form of nicotinamide adenine dinucleotide (NAD) [22]. Although the mitochondrial ETC is known to be the major source of cellular ROS, the KGDH complex can produce superoxide and hydrogen peroxide at eight times higher concentration compared with complex I [23]. Metabolic perturbation of αKG and NADH accumulation might result in KGDH complex-dependent oxidative stress and could profoundly affect the redox state of cancer cells [24]. Our study also showed a crucial role of DLD in ferroptosis induced by cystine deprivation or cystine import inhibition in cancer cells. Our evidence also implied that DLD gene silencing blocked lipid peroxidation and ferroptosis *in vitro* and *in vivo*. In contrast, DLST did not contribute to cystine deprivation-induced ferroptosis in cancer cells, although its reduction causes ROS generation and oxidative stress in neurodegeneration [25].

Cystine deprivation or import inhibition induces a transient hyperpolarization of MMP, followed by the eventual collapse leading to cell death. This was recently introduced as a unique feature of cystine deprivation-induced ferroptosis, indicative of the pivotal role of mitochondrial metabolic activity [15]. Lipid ROS accumulation appeared to accompany hyperpolarization of MMP. In our study, mitochondrial metabolic activity, which is a result of anaplerotic reactions that fuel the TCA cycle, may reflect the change in MMP. Damage of mitochondrial integrity and outer membrane permeabilization may also be observed in apoptosis, which would result in the release of mitochondrial regulatory proteins into the cytoplasm [26]. Both the present and previous studies [15] have revealed that the mitochondria plays a proactive role in ferroptosis by fueling both metabolic pathway and inducing lipid ROS production.

The present study demonstrated that cystine deprivation caused iron starvation response and mitochondrial iron accumulation in cancer cells. Aconitase is an enzyme catalyzing the production of isocitrate from citrate in the TCA cycle and has an association with ROS sensitivity [27]. Aconitase, a mitochondrial iron sulfur cluster (ISC) protein, acts as an iron-responsive element in its oxidized form, which can regulate the translation of cellular proteins, such as transferrin receptor, ferritin, and ferroportin [28]. Therefore, aconitase may cause iron- and ROS-mediated cellular toxicity [29,30]. In our study, cystine deprivation not only decreased the functional activity of aconitase but also induced iron starvation response. This ultimately resulted in an increased intracellular free iron level and ferrous iron accumulation in the mitochondria, which are prerequisites of Fenton reaction for ferroptosis. Cysteine and GSH depletion arising from cystine deprivation reportedly affect biosynthesis, storage, and trafficking of mitochondrial ISCs as well as reduce the extent of cellular ROS removal [31]. Recently, the loss of mitochondrial ISCs combined with cystine deprivation was found to upregulate iron starvation response, increase transferrin receptor level, and decrease ferritin level, thereby resulting in an increased intracellular free iron content and ferroptosis induction [32]. Contrastingly, fumarate accumulation and malate depletion in cancer cells with fumarate hydratase deficiency inhibit aconitase activity for ISC binding, thereby contributing to the dysregulated metabolism in cancer cells [33]. A recent study has also reported that loss-of-function mutation of fumarate hydratase prevents cystine deprivation-induced ferroptosis [15].

Analyses of the HNC cohort in the TCGA datasets revealed that DLD mRNA expression was lower in cancer cells than in normal cells but had no association with survival. Human cancer cells express DLD at a lower level than that expressed by normal cells, and such a low expression is related to poor survival outcomes in several types of cancers, including renal cancer, colon cancer, cervical cancer [34]. The same results have been observed with regard to the expression of ACO1 and ACO2 in human cancers [34]. Cancer cells exhibit higher ROS levels (retained at an upper threshold) than healthy cells [35]. The vulnerability of cancer cells to oxidative stress is the “Achilles heel,” and ROS modulation in cancer cells has become a popular strategy for anticancer therapy [36]. In line with this observation, a recent study showed that the integrin-mediated delivery of bioengineered ROS-generating DLD effectively targeted melanoma cells and spared the healthy cells [37].

5. Conclusion

This study suggests that DLD is closely linked to ferroptosis induced by cystine deprivation or import inhibition. Cystine deprivation and glutaminolysis increase mitochondrial KGDH activity, MMP, and ferrous iron level, leading to mitochondrial lipid peroxidation and ferrous iron accumulation. Cystine deprivation also induces iron starvation response responsible for boosting up cellular free iron level, which in turn results in Fenton reaction and ferroptosis (Fig. 7).

Author contributions

Daiha Shin and Jong-Lyel Roh conceived and designed the experiments. Daiha Shin, Jaewang Lee, Ji Hyeon You, Doyeon Kim, and Jong-Lyel Roh performed the experiments. Daiha Shin and Jong-Lyel Roh analyzed the data. Daiha Shin, Jaewang Lee, Ji Hyeon You, and Doyeon Kim contributed reagents/materials/analysis tools; Daiha Shin and

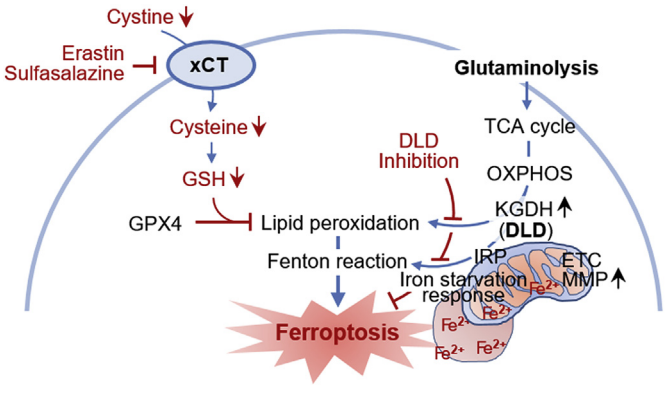

Fig. 7. A schematic showing a close relationship between DLD and cystine deprivation- or import inhibition-induced ferroptosis. Cystine deprivation and glutaminolysis increases mitochondrial α-ketoglutarate dehydrogenase (KGDH) activity, membrane potential (MMP), and ferrous iron content. This leads to lipid peroxidation accumulation and Fenton reaction which cause ferroptosis. DLD inhibition decreases both lipid peroxidation and ferrous iron accumulation, resulting in ferroptosis suppression.

Jong-Lyel Roh wrote the draft, and checked and revised. All authors approved to submit this version to this publication.

Declaration of competing interest

All authors declare no conflict of interests.

Acknowledgements

This study was supported by the National Research Foundation of Korea (NRF) grant, funded by the Ministry of Science and ICT (MSIT), The Government of Korea (No. 2019R1A2C2002259) (J.-L. Roh).

Appendix A. Supplementary data

Supplementary data to this article can be found online at https://doi.org/10.1016/j.redox.2019.101418.

Transparency document

Transparency document related to this article can be found online at https://doi.org/10.1016/j.redox.2019.101418

References

[1] B.R. Stockwell, J.P. Friedmann Angeli, H. Bayir, A.I. Bush, M. Conrad, S.J. Dixon, S. Fulda, S. Gascon, S.K. Hatzios, V.E. Kagan, K. Noel, X. Jiang, A. Linkermann, M.E. Murphy, M. Overholtzer, A. Oyagi, G.C. Pagnussat, J. Park, Q. Ran, C.S. Rosenfeld, K. Salnikow, D. Tang, F.M. Torti, S.V. Torti, S. Toyokuni, K.A. Woerpel, D.D. Zhang, Ferroptosis: a regulated cell death nexus linking metabolism, redox biology, and disease, Cell 171 (2017) 273–285.

[2] K. Shimada, R. Skouta, A. Kaplan, W.S. Yang, M. Hayano, S.J. Dixon, L.M. Brown, C.A. Valenzuela, A.J. Wolpaw, B.R. Stockwell, Global survey of cell death mechanisms reveals metabolic regulation of ferroptosis, Nat. Chem. Biol. 12 (2016) 497–503.

[3] J.P.F. Angeli, R. Shah, D.A. Pratt, M. Conrad, Ferroptosis inhibition: mechanisms and opportunities, Trends Pharmacol. Sci. 38 (2017) 489–498.

[4] V.E. Kagan, G. Mao, F. Qu, J.P. Angeli, S. Doll, C.S. Croix, H.H. Dar, B. Liu, V.A. Tyurin, V.B. Ritov, A.A. Kapralov, A.A. Amoscato, J. Jiang, T. Anthonymuthu, D. Mohammadyani, Q. Yang, B. Proneth, J. Klein-Seetharaman, S. Watkins, I. Bahar, J. Greenberger, R.K. Mallampalli, B.R. Stockwell, Y.Y. Tyurina, M. Conrad, H. Bayir, Oxidized arachidonic and adrenic PEs navigate cells to ferroptosis, Nat. Chem. Biol. 13 (2017) 81–90.

[5] S. Doll, B. Proneth, Y.Y. Tyurina, E. Panzilius, S. Kobayashi, I. Ingold, M. Irmler, J. Beckers, M. Aichler, A. Walch, H. Prokisch, D. Trumbach, G. Mao, F. Qu, H. Bayir, J. Fullekrug, C.H. Scheel, W. Wurst, J.A. Schick, V.E. Kagan, J.P. Angeli, M. Conrad, ACSL4 dictates ferroptosis sensitivity by shaping cellular lipid composition, Nat. Chem. Biol. 13 (2017) 91–98.

[6] W. Hou, Y. Xie, X. Song, X. Sun, M.T. Lotze, H.J. Zeh 3rd, R. Kang, D. Tang, Autophagy promotes ferroptosis by degradation of ferritin, Autophagy 12 (2016) 1425–1428.

[7] B. Zhou, J. Liu, R. Kang, D.J. Klionsky, G. Kroemer, D. Tang, Ferroptosis is a type of autophagy-dependent cell death, Semin. Cancer Biol. (2019) E-pub.

[8] L. Galluzzi, I. Vitale, S.A. Aaronson, J.M. Abrams, D. Adam, P. Agostinis, E.S. Alnemri, L. Altucci, I. Amelio, D.W. Andrews, M. Annicchiarico-Petruzzelli, A.V. Antonov, E. Arama, E.H. Baehrecke, N.A. Barlev, N.G. Bazan, F. Bernassola, M.J.M. Bertrand, K. Bianchi, M.V. Blagosklonny, K. Blomgren, C. Borner, P. Boya, C. Brenner, M. Campanella, E. Candi, D. Carmona-Gutierrez, F. Cecconi, F.K. Chan, N.S. Chandel, E.H. Cheng, J.E. Chipuk, J.A. Cidlowski, A. Ciechanover, G.M. Cohen, M. Conrad, J.R. Cubillos-Ruiz, P.E. Czabotar, V. D'Angiolella, T.M. Dawson, V.L. Dawson, V. De Laurenzi, R. De Maria, K.M. Debatin, R.J. DeBerardinis, M. Deshmukh, N. Di Daniele, F. Di Virgilio, V.M. Dixit, S.J. Dixon, C.S. Duckett, B.D. Dynlacht, W.S. El-Deiry, J.W. Elrod, G.M. Fimia, S. Fulda, A.J. Garcia-Saez, A.D. Garg, C. Garrido, E. Gavathiotis, P. Golstein, E. Gottlieb, D.R. Green, L.A. Greene, H. Gronemeyer, A. Gross, G. Hajnoczky, J.M. Hardwick, I.S. Harris, M.O. Hengartner, C. Hetz, H. Ichijo, M. Jaattela, B. Joseph, P.J. Jost, P.P. Juin, W.J. Kaiser, M. Karin, T. Kaufmann, O. Kepp, A. Kimchi, R.N. Kitsis, D.J. Klionsky, R.A. Knight, S. Kumar, S.W. Lee, J.J. Lemasters, B. Levine, A. Linkermann, S.A. Lipton, R.A. Lockshin, C. Lopez-Otin, S.W. Lowe, T. Luedde, E. Lugli, M. MacFarlane, F. Madeo, M. Malewicz, W. Malorni, G. Manic, J.C. Marine, S.J. Martin, J.C. Martinou, J.P. Medema, P. Mehlen, P. Meier, S. Melino, E.A. Miao, J.D. Molkentin, U.M. Moll, C. Munoz-Pinedo, S. Nagata, G. Nunez, A. Oberst, M. Oren, M. Overholtzer, M. Pagano, T. Panaretakis, M. Pasparakis, J.M. Penninger, D.M. Pereira, S. Pervaiz, M.E. Peter, M. Piacentini, P. Pinton, J.H.M. Prehn, H. Puthalakath, G.A. Rabinovich, M. Rehm, R. Rizzuto, C.M.P. Rodrigues, D.C. Rubinsztein, T. Rudel, K.M. Ryan, E. Sayan, L. Scorrano, F. Shao, Y. Shi, J. Silke, H.U. Simon, A. Sistigu, B.R. Stockwell, A. Strasser, G. Szabadkai, S.W.G. Tait, D. Tang, N. Tavernarakis, A. Thorburn, Y. Tsujimoto, B. Turk, T. Vanden Berghe, P. Vandenabeele, M.G. Vander Heiden, A. Villunger, H.W. Virgin, K.H. Vousden, D. Vucic, E.F. Wagner, H. Walczak, D. Wallach, Y. Wang, J.A. Wells, W. Wood, J. Yuan, Z. Zakeri, B. Zhivotovsky, L. Zitvogel, G. Melino, G. Kroemer, Molecular mechanisms of cell death: recommendations of the Nomenclature Committee on cell death 2018, Cell Death Differ. 25 (2018) 486–541.

[9] B. Hassannia, P. Vandenabeele, T. Vanden Berghe, Targeting ferroptosis to Iron Out Cancer, Cancer Cell 35 (6) (2019) 830–849 10.

[10] J.P. Friedmann Angeli, D.V. Krysko, M. Conrad, Ferroptosis at the crossroads of cancer-acquired drug resistance and immune evasion, Nat. Rev. Cancer 19 (7) (2019) 405–414.

[11] H. Feng, B.R. Stockwell, Unsolved mysteries: how does lipid peroxidation cause ferroptosis? PLoS Biol. 16 (2018) e2006203.

[12] P. Venditti, L. Di Stefano, S. Di Meo, Mitochondrial metabolism of reactive oxygen species, Mitochondrion 13 (2013) 71–82.

[13] S.W. Tait, A. Oberst, G. Quarato, S. Milasta, M. Haller, R. Wang, M. Karvela, G. Ichim, N. Yatim, M.L. Albert, G. Kidd, R. Wakefield, S. Frase, S. Krautwald, A. Linkermann, D.R. Green, Widespread mitochondrial depletion via mitophagy does not compromise necroptosis, Cell Rep. 5 (2013) 878–885.

[14] M. Gao, P. Monian, N. Quadri, R. Ramasamy, X. Jiang, Glutaminolysis and transferrin regulate ferroptosis, Mol. Cell 59 (2015) 298–308.

[15] M. Gao, J. Yi, J. Zhu, A.M. Minikes, P. Monian, C.B. Thompson, X. Jiang, Role of mitochondria in ferroptosis, Mol. Cell 73 (2019) 354–363 e353.

[16] J.S. Isaacs, Y.J. Jung, D.R. Mole, S. Lee, C. Torres-Cabala, Y.L. Chung, M. Merino, J. Trepel, B. Zbar, J. Toro, P.J. Ratcliffe, W.M. Linehan, L. Neckers, HIF overexpression correlates with biallelic loss of fumarate hydratase in renal cancer: novel role of fumarate in regulation of HIF stability, Cancer Cell 8 (2005) 143–153.

[17] S.Y. Kim, K.C. Chu, H.R. Lee, K.S. Lee, T.E. Carey, Establishment and characterization of nine new head and neck cancer cell lines, Acta Otolaryngol. 117 (1997) 775–784.

[18] T. Ishimoto, O. Nagano, T. Yae, M. Tamada, T. Motohara, H. Oshima, M. Oshima, T. Ikeda, R. Asaba, H. Yagi, T. Masuko, T. Shimizu, T. Ishikawa, K. Kai, E. Takahashi, Y. Imamura, Y. Baba, M. Ohmura, M. Suematsu, H. Baba, H. Saya, CD44 variant regulates redox status in cancer cells by stabilizing the xCT subunit of system xc(-) and thereby promotes tumor growth, Cancer Cell 19 (2011) 387–400.

[19] L. Jin, G.N. Alesi, S. Kang, Glutaminolysis as a target for cancer therapy, Oncogene 35 (2016) 3619–3625.

[20] M. Jennis, C.P. Kung, S. Basu, A. Budina-Kolomets, J.I. Leu, S. Khaku, J.P. Scott, K.Q. Cai, M.R. Campbell, D.K. Porter, X. Wang, D.A. Bell, X. Li, D.S. Garlick, Q. Liu, M. Hollstein, D.L. George, M.E. Murphy, An African-specific polymorphism in the TP53 gene impairs p53 tumor suppressor function in a mouse model, Genes Dev. 30 (2016) 918–930.

[21] R. Vatrinet, G. Leone, M. De Luise, G. Girolimetti, M. Vidone, G. Gasparre, A.M. Porcelli, The alpha-ketoglutarate dehydrogenase complex in cancer metabolic plasticity, Cancer Metabol. 5 (2017) 3.

[22] A.A. Starkov, G. Fiskum, C. Chinopoulos, B.J. Lorenzo, S.E. Browne, M.S. Patel, M.F. Beal, Mitochondrial alpha-ketoglutarate dehydrogenase complex generates reactive oxygen species, J. Neurosci. 24 (2004) 7779–7788.

[23] C.L. Quinlan, R.L. Goncalves, M. Hey-Mogensen, N. Yadava, V.I. Bunik, M.D. Brand, The 2-oxoacid dehydrogenase complexes in mitochondria can produce superoxide/hydrogen peroxide at much higher rates than complex I, J. Biol. Chem. 289 (2014) 8312–8325.

[24] V.I. Bunik, 2-Oxo acid dehydrogenase complexes in redox regulation, Eur. J. Biochem. 270 (2003) 1036–1042.

[25] M. Dumont, D.J. Ho, N.Y. Calingasan, H. Xu, G. Gibson, M.F. Beal, Mitochondrial dihydrolipoyl succinyltransferase deficiency accelerates amyloid pathology and memory deficit in a transgenic mouse model of amyloid deposition, Free Radic. Biol. Med. 47 (2009) 1019–1027.

[26] X. Jiang, X. Wang, Cytochrome C-mediated apoptosis, Annu. Rev. Biochem. 73 (2004) 87–106.

[27] A.C. Nulton-Persson, L.I. Szweda, Modulation of mitochondrial function by hydrogen peroxide, J. Biol. Chem. 276 (2001) 23357–23361.

[28] O.V. Lushchak, M. Piroddi, F. Galli, V.I. Lushchak, Aconitase post-translational modification as a key in linkage between Krebs cycle, iron homeostasis, redox signaling, and metabolism of reactive oxygen species, Redox Rep. 19 (2014) 8–15.

[29] D. Cantu, J. Schaack, M. Patel, Oxidative inactivation of mitochondrial aconitase results in iron and H2O2-mediated neurotoxicity in rat primary mesencephalic cultures, PLoS One 4 (2009) e7095.

[30] G. Esposito, M. Vos, S. Vilain, J. Swerts, J. De Sousa Valadas, S. Van Meensel, O. Schaap, P. Verstreken, Aconitase causes iron toxicity in Drosophila pink1 mutants, PLoS Genet. 9 (2013) e1003478.

[31] G. Calabrese, B. Morgan, J. Riemer, Mitochondrial glutathione: regulation and functions, Antioxidants Redox Signal. 27 (2017) 1162–1177.

[32] S.W. Alvarez, V.O. Sviderskiy, E.M. Terzi, T. Papagiannakopoulos, A.L. Moreira, S. Adams, D.M. Sabatini, K. Birsoy, R. Possemato, NFS1 undergoes positive selection in lung tumours and protects cells from ferroptosis, Nature 551 (2017) 639–643.

[33] N. Ternette, M. Yang, M. Laroyia, M. Kitagawa, L. O'Flaherty, K. Wolhulter, K. Igarashi, K. Saito, K. Kato, R. Fischer, A. Berquand, B.M. Kessler, T. Lappin, N. Frizzell, T. Soga, J. Adam, P.J. Pollard, Inhibition of mitochondrial aconitase by succination in fumarate hydratase deficiency, Cell Rep. 3 (2013) 689–700.

[34] The Human Protein Atlas. Version 18.1..

[35] C. Gorrini, I.S. Harris, T.W. Mak, Modulation of oxidative stress as an anticancer strategy, Nat. Rev. Drug Discov. 12 (2013) 931–947.

[36] D. Trachootham, J. Alexandre, P. Huang, Targeting cancer cells by ROS-mediated mechanisms: a radical therapeutic approach? Nat. Rev. Drug Discov. 8 (2009) 579–591.

[37] A. Dayan, G. Fleminger, O. Ashur-Fabian, Targeting the Achilles' heel of cancer cells via integrin-mediated delivery of ROS-generating dihydrolipoamide dehydrogenase, Oncogene 38 (25) (2019) 5050–5061.